Coordination-resolved local bond relaxation and electron binding-energy shift of Pb solid skins and atomic clusters

Maolin Bo, [a] Yan Wang,[b, *] Yongli Huang, [a] Wei Zhou,[a] Can Li, [c]

Chang Q Sun [d,*]

[a]Key Laboratory of Low-Dimensional Materials and Application Technologies, Ministry of Education, Xiangtan University, Hunan 411105, China

[b]School of Information and Electronic Engineering, Hunan University of Science and Technology, Hunan 411201, China

[c]Center for Coordination Bond and Electronic Engineering, School of Materials Science and Engineering, China Jiliang University, Hangzhou 330018, China

[d]School of Electrical and Electronic Engineering, Nanyang Technological University, Singapore 639798, Singapore

E-mail: YWang8@hnust.edu.cn; ecqsun@ntu.edu.sg

(CQ is associated with honorary appointments at rest affiliations)

Abstract

Lead (Pb) demonstrates an pronounced energy states pertaining to undercoordinated skin and edge atoms with the physical origin of these excessive states remains unclear. Here we show that consistency between Density Functional Theory calculations and photoelectron spectroscopy measurements confirmed our theoretical predications on the $5d$ core-level shift of Pb skins and clusters. It is clarified that the shorter and stronger bonds between undercoordinated atoms cause local densification and entrapment of the core electrons, which in turn polarize the otherwise conducting electrons in the skins and edges, resulting in the respective electron binding-energy shift. Numerical analysis turns out that the $5d_{5/2}$ level shifts from the value of 18.283 eV for an isolated Pb atom by 3.478 eV upon bulk formation. Meanwhile, this strategy has enabled determination of the local bond length, bond energy, binding energy density, and atomic cohesive energy at the undercoordinated atomic sites.

Keywords: Pb nanoclusters, XPS, DFT, binding energy, BOLS

1. Introduction

Solid skins and atomic clusters of a substance are of great importance because of their size dependence of known properties and size emergence of new features due to the unusual interaction between undercoordinated atoms[1]. The known bulk properties such as elastic modulus[2], dielectric constant[3], melting point[4], band gap[5], etc., keep no longer constant but change with solid size, or the fraction of undercoordinated atoms involved. As the size shrinks, a nanostructure also demonstrates properties that its bulk parent does not exhibit such as the dilute magnetism[6, 7], catalytic ability[8, 9], and creation of Dirac-Fermions for topological insulators[10, 11]. Such size dependency and size emergency laid the foundation of nanoscience and nanotechnology[12, 13]. The physical mechanism behind the size dependency and size emergency and the correlation among all detectable properties remain high challenge.

X-ray photoelectron spectroscopy (XPS) provides a powerful means for studying electronic binding energy of both solid skins[12, 14-19] and size-selected clusters of Pb[20-24] that forms an important component in the topological insulators, for instance. The energy shift of the core level fingerprints the interaction between atoms that drives the unusual behavior of the skin and atomic clusters. Generally, XPS collects information in the form of broad peaks representing the mixture of the bulk and the sublayers in the skin[25-28]. A free-electron laser ultraviolet (UPS) and XPS investigation of the size-selected clusters revealed a linear dependence of the energy shifts of the core band on the inverse of particle size[29-31]. Therefore, correlation between the XPS/UPS binding energy and the unusual properties demonstrated by skins and clusters is necessary.

In this paper, we report findings in the local bond relaxation and the associated electronic binding energy shift of Pb surfaces and atomic clusters gained from density-functional theory (DFT) calculations and XPS spectral analysis. Quantitative reproduction of the Pb $5d_{5/2}$ energy shifts revealed the essentiality of the undercoordination induced local bond contraction, quantum entrapment, and valence charge polarization, which verifies our predictions based on the BOLS (bond order-length-strength) correlation notation[32].

2. Principles and calculation methods

2.1 BOLS-TB notation

According to the band theory, the vth energy level of an isolated atom, $E_v(0)$, is determined by the integral of the intra-atomic potential, $V_{atom}(r)$, and the eigenwave function for electrons of an atom at the specific ith atomic site, $|v, i\rangle$. Upon the involvement of the inter-atomic potential $V_{cry}(r)$, the binding energy (BE) will shift from the origin $E_v(z = 0)$ to $E_v(z = 12)$ by an amount of $E_v(z = 12) - E_v(0)$ that is proportional to the cohesive energy per bond between atom with 12 neighbors of standard,

$$E_v(0) = \langle v,i|V_{atom}(r)|v,i\rangle$$

$$E_v(12) - E_v(0) = \langle v,i|V_{cry}(r)|v,i\rangle + \sum_{j=1}^{j=z}\langle v,i|V_{cry}(r)|v,j\rangle = \alpha(1+\frac{z\beta}{\alpha}) \cong \alpha \propto E_b$$

(1)

The coordination number (CN) $z = 0$ and 12 represents an isolated atom and an atom in the bulk, respectively. The sum is over all z neighbors of the specific ith atom. Because $\langle v,i|v,j\rangle = \delta_{ij}$ with δ_{ij} being the Koronig function (if $i = j$, $\delta_{ij} = 1$, otherwise, $\delta_{ij} = 0$), the term $z\beta/\alpha \ll 1$. Any perturbation to the bond energy E_b will shift the core level accordingly.

According to BOLS notation, atomic undercoordination shortens and strengthens the bond between undercoordinated atoms, which follow the relations, $d_i = C_z d_b = 2d_b / \{1 + \exp[(12 - z_i)/8z_i]\}$ and $E_i = C_z^{-m} E_b$, where C_z is the coefficient of bond contraction with z_i being the effective coordination number of an atom in the ith atomic layer. The i counts from the outermost atomic layer inward up to the third layer. The bond nature indicator m represents how the bond energy changes with bond length. For most metals, $m = 1$. Incorporating the TB approximation and BOLS correlation with inclusion of the polarization turns out,

$$V_{cry}(\Delta_H) = V_{cry}(r)[1 + \Delta_H]$$

$$\Delta_H = \begin{cases} C_z^{-m} - 1 & (Entrapment\,(Surface)) \\ \tau K^{-1} \sum_{\le 3} C_z (C_z^{-m} - 1) & (Entrapment\,(Clusters)) \\ (E_v(p) - E_v(0)) / ((E_v(12) - E_v(0))) - 1 & (Porlarization) \end{cases}$$

$$(2)$$

The P and T represent the polarization and entrapment as illustrated in Fig 1. The shape factor $\tau =$ 1, 2, and 3 corresponds to a thin plate, a cylindrical rod, and a sphere dot, respectively. $K = R/d_b$ being the dimensionless form of size is the number of atoms lined along the radius of a spherical nanoparticle.
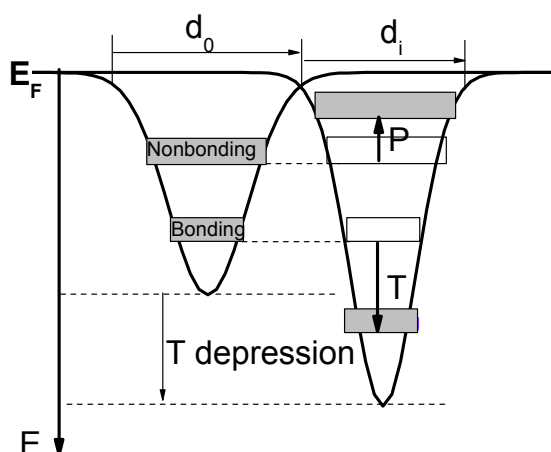
Figure 1   Schematic illustration of the atomic under-coordination induced local bond contraction ($d_z < d_0$), the associated quantum entrapment (T) and the polarization of the nonbonding states (P) by the densely entrapped bonding and core charges. This sequence of processes modulates the Hamiltonian by crystal potential splitting and charge distribution in all bands.

With respect to the bulk shift $\Delta E_v(12)$, the under-coordination induced core level shifts (CLSs), $\Delta E_v(z)$, follows:

$$\frac{\Delta E_v(z)}{\Delta E_v(12)} = \frac{E_v(z) - E_v(0)}{E_v(12) - E_v(0)} = \frac{E_z}{E_b} = C_z^{-1} = 1 + \Delta_H$$

$$(3)$$

With the given energies of the surface XPS spectral components related to z and z' coordination numbers and their correlation, we can determine the referential $E_v(0)$, the bulk shift, $\Delta E_v(12)$, and the z dependent shift:

$$\frac{E_v(z) - E_v(0)}{E_v(z') - E_v(0)} = \frac{C_z^{-1}}{C_{z'}^{-1}} \ (z' \neq z) \ \ or \ E_v(0) = \frac{C_{z'} E_v(z') - C_z E_v(z)}{C_{z'} - C_z} \ \ (z' \neq z)$$

$$E_v(z) - E_v(0) = \left[E_v(12) - E_v(0) \right] \times C_z^{-1}$$

(4)

Using the sum rule of the core−shell structure and taking the surface-to-volume ratio into account, we can deduce the K dependence of vth energy level $E_v(0)$ and its bulk shift $\Delta E_v(12)$:

$$E_v(K) = E_v(12) + \left[E_v(12) - E_v(0) \right] \times \Delta_H$$

(5)

Generally, the size-induced BE shifts for nanoparticles depends inversely on the size in the form of, $E_v(K) = A + BK^{-1}$, where A and B are constants that can be determined by finding the intercept and the gradient of the $E_v(K)$ line. Comparing the experimental scaling relationship with the theoretical expression in Eq(5) yields,

$$\begin{cases} A = E_v(12) \\ B = \left[E_v(12) - E_v(0) \right] \times \tau \sum_{i \leq 3} C_z (C_z^{-m} - 1) \end{cases}$$

(6)

With the derived $E_v(12)$, $E_v(0)$, and the given z values for the outermost three atomic layers, we are able to decompose the measured XPS spectra into the corresponding surface and bulk components.

The BOLS notation agrees with the latest model[33] of surface potential trap which indicates that the charge in the skin is higher and the potential trap is deeper than in the bulk.

2.2 Computational details

In order to verify our BOLS-TB predictions, we conducted first-principles DFT calculations on the optimal Pb_N clusters[34-36], as shown in Fig 2. Calculations were focused on the change of bond and electronic characteristics of under-coordinated atoms, geometric structures and size dependence, the charge transfer using Mulliken population analysis, and the energetic distribution of the core band and valence states. The relativistic DFT calculations were conducted using the DMol3 code with a double numeric plus polarization basis set[37]. The treatment of core electrons considered by the DFT semi-core pseudopotential[38]. The DFT exchange-correlation potential utilized the local-density approximation (LDA), with the PWC function for geometry and electronic structures[39]. During calculations, the self-consistency threshold of the total energy was set at 10^{-6}au. The tolerance limit for the energy, forces and displacement in geometry optimizations were set, respectively, at 10^{-5} Hartree, 0.002 Hartree/Å and 0.005 Å, respectively. The calculations presented in this paper have been performed with spin-polarized code for Pb edge states[40].

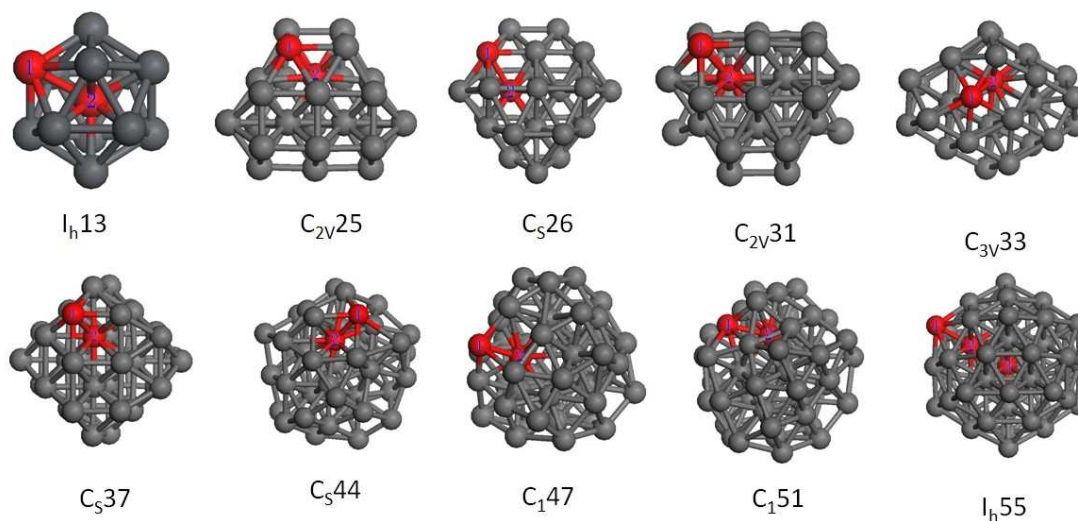Figure 2 Pb_N geometric structures optimized based on the initial configurations of J.P.K Doye and S.C Hendy using Gupta and Glue potentials.[35, 36]

3.   Results and Discussion

3.1 Atomic coordination - resolved quantum entrapment

Each XPS spectrum is decomposed into components corresponding to the bulk (B) and surface skins (S_i) from higher (smaller value) to lower BE upon background correction[41]. The

number of components is taken with respect to the originally reported count. The peak energies are subject to refinement by fitting the overall convoluted peak intensity. On the framework of the BOLS-TB approaches, we decomposed the XPS $5d_{5/2}$ spectra collected from clean Pb surfaces[14, 15] and atomic clusters [20] (see Fig 3 and Table 1).

Table 1 Effective atomic CN (z), lattice strain ($\varepsilon_z = C_z$-1 (%)), relative BE shift ($\delta E_z = \Delta E(z)/\Delta E(12)-1 = (C_z^{-1}-1)(\%)$), **relative atomic cohesive energy ($E_c = E_c(z)/E_c(12)$-1= $(z_{ib}C_z^{-1}-1)(\%)$), and the relative BE density ($E_D = E_D(z)/E_D(12)= (C_z^{-4}-1)(\%)$)** in various registries of Pb skins. $E_V = 0$ is taken as the reference.

	i	z	$5d_{5/2}$(eV)	$-\varepsilon_z$ (%)	δE_z (%)	δE_D (%)	$-\delta E_C$ (%)
$E_v(0)$	-	0	18. 283	-	-	-	-
$E_v(12)$	B	12	21. 761	0	0	0	0
$\Delta E_v(12)$	-	-	3.478	-	-	-	-
Pb (111)	S_2	6. 28	18. 065(E_F)	5. 63	5. 97	26. 09	44. 54
	S_1	4. 26	18. 304(E_F)	11. 31	12. 75	61. 63	59. 97
Pb/Si (100)	S_2	5. 73	18. 020(E_F)	6. 83	7. 33	32. 71	48. 75
	S_1	4	18. 254(E_F)	12. 44	14. 21	70. 13	61. 93
Pb (n = 3000)	S_2	3. 69	22. 325	13. 97	16. 24	82. 56	64. 26
	S_1	2. 45	22. 855	23. 93	31. 46	198. 64	73. 16
Pb (n = 1000)	S_2	3. 47	22. 387	15. 27	18. 02	94. 02	65. 87
	S_1	2. 37	22. 910	24. 84	33. 05	213. 37	73. 72

The spectra were decomposed into the B, the first, and the second (S_1, S_2) atomic layers of the surface. Including the common B component (z = 12), there are a total of $l=5$ components for these two surfaces. There will be a combination of $N=C_l^2 =l!/[(l-2)!2!]$ 10

values of $E_v(0)$. Using the least-root-mean-square approach, we can find the average of $\langle E_v(0) \rangle = \sum_N \langle E_{vi}(0) \rangle / N$ and the standard deviation. A fine tuning of the CN values of the components will minimize the σ and improve the accuracy of the effective CN for each sublayer, and hence to determine the local strain, the BE density, and the cohesive energy per discrete atom in differently oriented surface layers. With the derived z value and the $5d_{5/2}$ BE for each XPS component, one is able to predict the z-resolved local lattice strain, BE shift, atomic cohesive energy E_C and binding energy density E_D in the Pb surface skins, as shown in Fig 4 and Table 1, where $z_{ib} = z/12$ is the reduced CN, $z = 12$ is the bulk value.
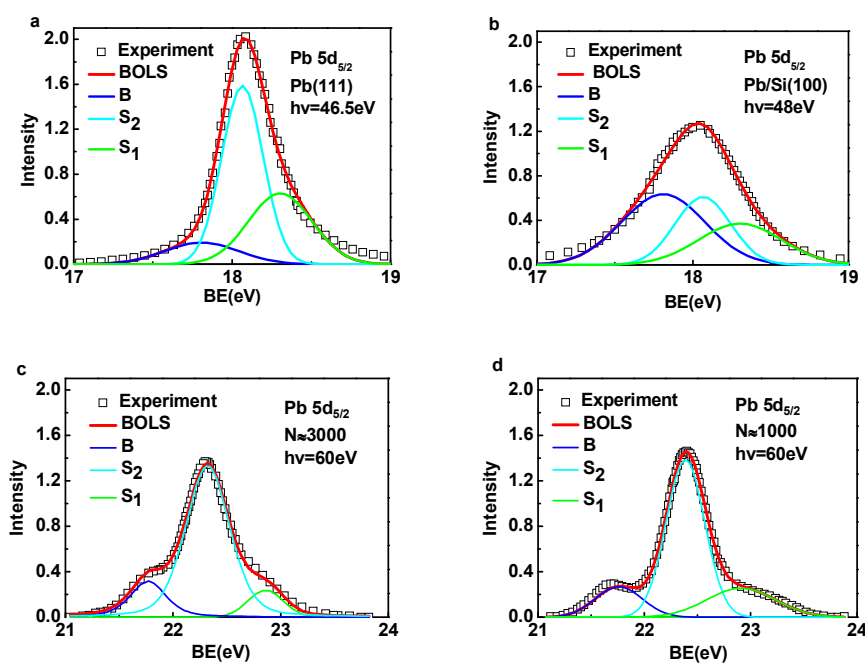

Figure 3 Decomposition of (a) the Pb $5d_{5/2}$ spectra for the (111) skin[15] (b) Pb film on Si substrate[14], and (c, d) atomic clusters[20] with three Gaussian components representing the bulk B, S_2, and S_1 states from higher to lower BE. Table 1 features the derived information.
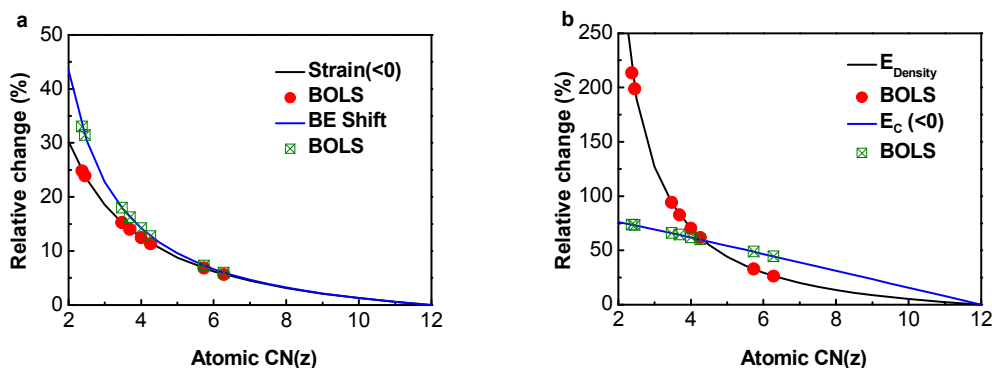
Figure 4 Coordination number (z) resolved (a) local bond strain and BE shift (entrapment); and, (b) atomic

cohesive energy E_C and binding energy density E_D.

The E_v (0) and E_v (12) are intrinsic constants, disregarding the coordination and chemical environment of a given material. Using the least-root-mean-square approach, we obtained the z-resolved $5d_{5/2}$ core-level shift for Pb skins and atomic clusters:

$$
\begin{cases}
E_{5d_{5/2}}(C_z) = \left\langle E'_{5d_{5/2}}(0) \right\rangle \pm \sigma + \Delta E_{5d_{5/2}}(B)C_z^{-m} = 14.334 \pm 0.005 + 3.475 C_z^{-1} & \text{(Fermi level)} \\
E_{5d_{5/2}}(C_z) = \left\langle E_{5d_{5/2}}(0) \right\rangle \pm \sigma + \Delta E_{5d_{5/2}}(B)C_z^{-m} = 18.283 \pm 0.002 + 3.478 C_z^{-1} & \text{(Vacuum level)}
\end{cases}
$$

The binding energies can be referred either to the vacuum level or the Fermi level. of the difference between these reference points is the work function $E_{5d_{5/2}}(0) - E'_{5d_{5/2}}(0) = 3.951$ eV, which is sufficiently accurate compared with direct measurements[21].

3.2 Bond contraction and nonbonding electron polarization(NEP)

Consistency in the BOLS-TB analysis of the XPS spectra and DFT calculations confirms the BOLS-TB predictions of the spontaneous bond contraction in the Pb solid skins and atomic clusters disregarding the sizes and structures used in the calculations. In fact, the highly coordinated atoms prefer larger first-neighbor distances than the undercoordinated ones. Therefore, atoms in the cluster interior exhibits the ideal distance of the bulk fcc crystal, while skin atoms show bond contraction. Results obtained here agree with the reported bond contraction occurring in Ag, Au, Cu, Ni, Pd, Pt, Fe atomic chains[42, 43] with clarification of the quantum entrapment and polarization in this contribution.

The spontaneous process of bond contraction and strengthening will cause local

densification and quantum entrapment of bonding charge and binding energy. Table 2 features the charge flow with the clusters estimated using the Mulliken population analysis. Results indicate that electrons flow from the inner to the outermost layer of the clusters. Fig 5a shows the *d*-orbit local DOS for Pb I_h13 and I_h55 structures. Globally positive CLS happens as the Pb cluster sizes are reduced because of the undercoordination induced quantum entrapment, and hence the positive core level shift results.

According to the BOLS-NEP notation,the originally conductive *p*-electrons of Pb are expected to be polarized and locally-pinned by the densely- and tightly-trapped core charges. These polarized and unpaired electrons neither follow the regular dispersion relation nor occupy the allowed energy states in the valence band and below as defined by the Hamiltonian.Finally, the polarized and unpaired electrons with non-zero spin will in turn screen and split the crystal potential and consequently generate extra component in the upper edge of the core band. Fig 5b shows that the LDOS moves to the upper edge near the $E_f(=0)$, and the smallest cluster moves most. The valence electrons also move up towards E_f as the sizes of Pb clusters decrease.

Table 2   Bond length (d_i), bond strain (C_z-1), and charge transfer with Pb_N clusters. Charge flows from the inner to the outermost atomic shells due to the BOLS-NEP effect. Negative sign means charge gain otherwise charge loss.

Structure	d_{12}(Å) (position1-2)	C_z-1(%)	Charge Transfer(*e*) (Shell layer1-2)	CLS ($E_v(N)-E_v(0)$)
I_h 13	3. 195	-8. 714	-0. 817	2. 98
$C_{2V}25$	3. 111	-11. 114	-1. 564	2. 71
C_S26	3. 102	-11. 371	-1. 532	2. 67
$C_{2V}31$	3. 104	-11. 314	-1. 453	2. 66
$C_1 33$	3. 120	-10. 857	-1. 547	2. 63
$C_{3V}37$	3. 127	-10. 657	-1. 764	2. 57
C_S44	3. 102	-11. 371	-2. 241	2. 54

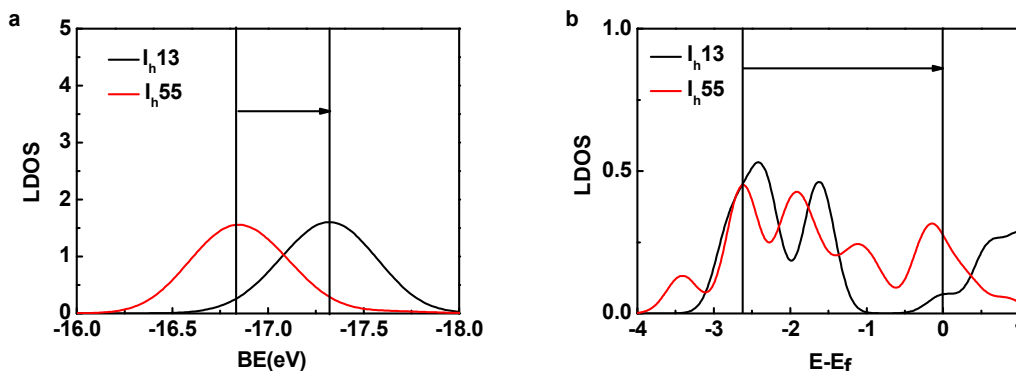|				
$C_1 47$	3. 114	-11. 029	-2. 063	2. 53
$C_1 51$	3. 110	-11. 143	-2. 068	2. 52
I_h 55	3. 155	-9. 857	-2. 454	2. 49

Figure 5   Undercoordination induced (a) core band quantum entrapment and (b) valence band

polarization of Pb I_h13 and I_h55 clusters.

Calculations confirmed the BOLS-NEP expected lattice strain, charge transfer in real space from the inner to the outermost atomic shell, and valence charge polarization from the lower to the higher binding energies of the well defined Pb clusters. Bonds between the lower coordinated atoms at corners or at edges contract more significantly than those in the cluster interior.

3.3 Size-resolved quantum entrapment

If a cluster is approximately spherical, the number of atoms N is related to its radius K by,

$$N = 4\pi K^3 / 3$$
$$K^{-1} = (3N / 4\pi)^{-1/3} = 1.29 N^{-1/3}$$

(7)

Eq (6) yields the N-dependence of the core level BE:

$$E_v(N) = E_v(12) + \Delta E_v(12)\left[1.29\tau N^{-1/3}\sum_{i\leq 3} C_z\left(C_z^{-m} - 1\right)\right]$$

$$(8)$$

As in the BOLS convention, choosing Pb (n = 1000) cluster for the standard reference, thus z_1 = 2.37 and z_2 = 3.47. From the relation of $C(z_i)$ in $d_i = C_z d_b = 2d_b / \{1 + \exp[(12 - z_i)/8z_i]\}$, C_1, C_2, were calculated to be 0.7514 and 0.8476, respectively, from which $\Delta_{1,2}$ = 0.1868 and 0.1292. The sum of $\Delta_H = \Delta_1 + \Delta_2 \approx 0.3160$. With the value of $\Delta E_{5d5/2}(12)$ derived from surface analysis, we can calculate the BE change without needing any other assumptions:

$$\begin{cases} E_v(N) = E_v(12) + 1.418\tau N^{-1/3}(\text{eV}) & (\text{Experimental}) \\ E_v(N) = E_v(12)' + \Phi + 1.418\tau N^{-1/3}(\text{eV}) & (\text{Calculation}) \end{cases}$$

and hence,

$$\begin{cases} \Phi = E_v(12) - E_v(12)'(\text{eV}) \\ \Phi = \Phi_1 + \left(E_v(N) - E_v(12)'\right)(\text{eV}) \end{cases}$$

$$(9)$$

Fig 6 shows that BE increases linearly with $N^{-1/3}$, we can then determine the shape factor τ = 2.52 and Φ = 1.94 eV. The principle of Eq(9), Φ is the Bulk value difference between DFT calculation and experimental. Derived from the DFT calculation data $\Delta E_v(N) = E_v(N) - E_v(12)'$ is mainly attributed to size contribution, and Φ_1 is BE difference between DFT calculation and experimental from Fermi level.
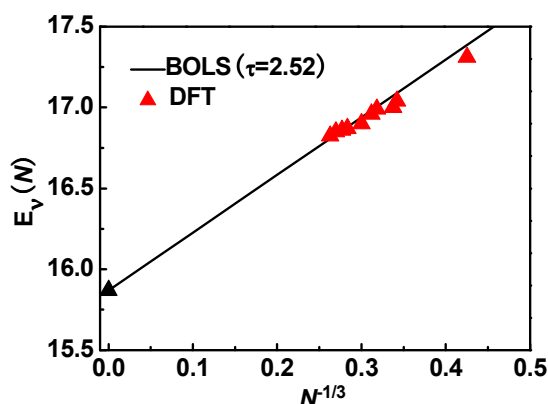

Figure 6 The $5d$ core band core level shift of size-selected free Pb_N clusters, are plotted versus $N^{-1/3}$.

The DFT calculation size trend of the energy shift is in consistence with the surface positive shift. Therefore, both the size- and the surface-induced energy shifts of Pb surfaces and atomic clusters are dominated by the shorter and stronger bonds between undercoordinated atoms result in positive core level shift and the skin-depth quantum entrapment.

4. Conclusion

Incorporating the BOLS-TB-NEP premise with the DFT calculations and XPS measurements has led to a consistent insight into the physical origin of the localized edge states of Pb skins and atomic clusters. Analyzing the XPS spectra for the Pb atomic clusters has resulted in the BE for an isolated atom as 18.283 eV and its bulk shift of 3.478 eV. It is clarified that the skin- and size-induced BE shift arise from the undercoordination-induced local strain and quantum entrapment. DFT calculations confirmed the BOLS-NEP expected the local bond contraction, nonbonding electrons polarization by the deeply and densely entrapped core and bonding electrons at edge boundary because of the shorter and stronger bonds between undercoordinated atoms.

References

1.   C. Q. Sun, *Relaxation of the Chemical Bond*. (Heidelberg New York Dordrecht London Singapore 2014).
2.   M. T. McDowell, A. M. Leach and K. Gall, Nano letters **8** (11), 3613-3618 (2008).
3.   H. Z. Guo, Y. Mudryk, M. I. Ahmad, X. C. Pang, L. Zhao, M. Akinc, V. K. Pecharsky, N. Bowler, Z. Q. Lin and X. Tan, Journal of Materials Chemistry, 23944-23951 (2012).
4.   W. H. Qi and M. P. Wang, Materials Chemistry and Physics **88** (2–3), 280-284 (2004).
5.   H. Xu, R. Q. Zhang, X. Zhang, A. L. Rosa and T. Frauenheim, Nanotechnology **18** (48), 485713-485713 (2007).
6.   P. Sahoo, H. Djieutedjeu and P. F. P. Poudeu, Journal of Materials Chemistry A **1** (47), 15022–15030 (2013).
7.   G. L. Nealon, B. Donnio, R. Greget, J. P. Kappler, E. Terazzi and J. L. Gallani, Nanoscale **4** (17), 5244-5258 (2012).

8.   I. B. Tsvetkova, V. G. Matveeva, V. Y. Doluda, A. V. Bykov, A. I. Sidorov, S. V. Schennikov, M. G. Sulman, P. M. Valetsky, B. D. Stein, C.-H. Chen, E. M. Sulman and L. M. Bronstein, Journal of Materials Chemistry **22** (13), 6441–6448 (2012).

9.   Z. Zhang, C. Shao, Y. Sun, J. Mu, M. Zhang, P. Zhang, Z. Guo, P. Liang, C. Wang and Y. Liu, Journal of Materials Chemistry **22** (4), 1387-1395 (2012).

10. C. Niu, Y. Dai, M. Guo, Y. Ma, B. Huang and M.-H. Whangbo, Journal of Materials Chemistry C **1** (1), 114–120 (2013).

11. R. J. Cava, H. Ji, M. K. Fuccillo, Q. D. Gibson and Y. S. Hor, Journal of Materials Chemistry C **1** (19), 3176-3189 (2013).

12. M. Özer, Y. Jia, B. Wu, Z. Zhang and H. Weitering, Physical Review B **72** (11), 113409-113409 (2005).

13. X.-Q. Zhang, E. Iype, S. V. Nedea, A. P. J. Jansen, B. M. Szyja, E. J. M. Hensen and R. A. van Santen, The Journal of Physical Chemistry C **118** (13), 6882-6886 (2014).

14. G. Le Lay, K. Hricovini and J. Bonnet, Physical Review B **39** (6), 3927-3930 (1989).

15. J. Dalmas, H. Oughaddou, G. Le Lay, B. Aufray, G. Tréglia, C. Girardeaux, J. Bernardini, J. Fujii and G. Panaccione, Surface Science **600** (6), 1227-1230 (2006).

16. R. W. Joyner, K. Kishi and M. W. Roberts, Proceedings of the Royal Society A: Mathematical, Physical and Engineering Sciences **358** (1693), 223-241 (1978).

17. K. Gürtler, K. Tan, G. Bancroft and P. Norton, Physical Review B **35** (12), 6024-6028 (1987).

18. M. C. Xu, H. J. Qian, F. Q. Liu, K. Ibrahim, W. Y. Lai and S. C. Wu, Solid State Communications **117** (5), 327-332 (2001).

19. D. J. Payne, R. G. Egdell, D. S. L. Law, P.-A. Glans, T. Learmonth, K. E. Smith, J. Guo, A. Walsh and G. W. Watson, Journal of Materials Chemistry **17** (3), 267-277 (2007).

20. S. Peredkov, S. Sorensen, A. Rosso, G. Öhrwall, M. Lundwall, T. Rander, A. Lindblad, H. Bergersen, W. Pokapanich, S. Svensson, O. Björneholm, N. Mårtensson and M. Tchaplyguine, Physical Review B **76** (8), 081402-081402 (2007).

21. D. Iablonskyi, M. Patanen, S. Aksela and H. Aksela, Physical Review B **86** (4), 041101-041101 (2012).

22. C. Zhang, T. Andersson, S. Svensson, O. Björneholm and M. Tchaplyguine, Physical Review B **87** (3), 035402-035402 (2013).

23. H. R. Siekmann, E. Holub-Krappe, B. Wrenger, C. Pettenkofer and K. H. Meiwes-Broer, Z. Physik B - Condensed Matter **90** (2), 201-206 (1993).

24. J. Bahn, P. Oelßner, M. Köther, C. Braun, V. Senz, S. Palutke, M. Martins, E. Rühl, G. Ganteför, T. Möller, B. von Issendorff, D. Bauer, J. Tiggesbäumker and K. H. Meiwes-Broer, New Journal of Physics **14** (7), 075008-075008 (2012).

25. J. Andersen, D. Hennig, E. Lundgren, M. Methfessel, R. Nyholm and M. Scheffler, Physical Review B **50** (23), 17525-17533 (1994).

26. M. Patanen, C. Nicolas, X. J. Liu, O. Travnikova and C. Miron, Physical Chemistry Chemical Physics **15** (25), 10112-10117 (2013).

27. D. M. Riffe and G. K. Wertheim, Physical Review B **47** (11), 6672-6679 (1993).

28. S. Lizzit, A. Baraldi, A. Groso, K. Reuter, M. V. Ganduglia-Pirovano, C. Stampfl, M. Scheffler, M. Stichler, C. Keller, W. Wurth and D. Menzel, Physical Review B **63** (20), 205419-205419 (2001).

29. M. Vogel, C. Kasigkeit, K. Hirsch, A. Langenberg, J. Rittmann, V. Zamudio-Bayer, A. Kulesza, R. Mitrić, T. Möller, B. v. Issendorff and J. Lau, Physical Review B **85** (19), 195454-195454 (2012).

30. K. Kooser, D. T. Ha, E. Itala, J. Laksman, S. Urpelainen and E. Kukk, The Journal of Chemical Physics **137** (4), 044304-044304 (2012).

31. S. Urpelainen, M. Tchaplyguine, M. H. Mikkelä, K. Kooser, T. Andersson, C. Zhang, E. Kukk, O. Björneholm and M. Huttula, Physical Review B **87** (3), 035411-035411 (2013).

32. C. Q. Sun, Physical Review B **69,** (4), 045105-045105 (2004).

33. L. Wan, S. Xu, M. Liao, C. Liu and P. Sheng, Physical Review X **4** (1), 011042 (2014).

34. B. Wang, J. Zhao, X. Chen, D. Shi and G. Wang, Physical Review A **71** (3), 033201-033201 (2005).

35. J. P. K. Doye, Computational Materials Science **35** (3), 227-231 (2006).

36. J. P. K. Doye and S. C. Hendy, The European Physical Journal D **22** (1), 99-107 (2003).

37. B. Delley, The Journal of Chemical Physics **92** (1), 508-517 (1990).

38. B. Delley, Physical Review B **66** (15), 155125-155125 (2002).

39. J. P. Perdew and Y. Wang, Physical Review B **45** (23), 13244-13249 (1992).

40. H. Li, Y. Ji, F. Wang, S. F. Li, Q. Sun and Y. Jia, Physical Review B **83** (7), 075429-075429 (2011).

41. Y. Wang, Y. G. Nie, J. S. Pan, L. K. Pan, Z. Sun, L. L. Wang and C. Q. Sun, Physical Chemistry Chemical Physics **12** (9), 2177-2182 (2010).

42. A. Kara and T. S. Rahman, Physical Review Letters **81** (7), 1453-1456 (1998).

43. F. Baletto, R. Ferrando, A. Fortunelli, F. Montalenti and C. Mottet, The Journal of Chemical Physics **116** (9), 3856-3863 (2002).